Measurement and Perturbation of Morphogen Lifetime: Effects on Gradient Shape

Jeffrey A. Drocco,[†‡] Oliver Grimm,[§] David W. Tank,[†§] Eric Wieschaus[§¶]

[†]Lewis-Sigler Institute for Integrative Genomics, [‡]Joseph Henry Laboratories of Physics, [§]Department of Molecular Biology, and [¶]Howard Hughes Medical Institute, Princeton University, Princeton, New Jersey

Supporting Material

S1 Table of symbols

Symbol	Description
I_{trans}	excitation beam intensity measured by trans-side PMT
I_{fluor}	pointwise fluorescence intensity measured by green channel epi-side PMT
η	calibrated offset for trans-side PMT
P	power of transmitted excitation beam, corrected for PMT offset, $P = I_{trans} - \eta$, used to normalized I_{fluor}
k_{off}/k_{on}	measured rates of Dronpa dark-conversion/reactivation
ξ	fraction of dark state Dronpa-Bcd reactivated by a 405 nm photoactivation series, $\xi = 98\%$
Q_{Bcd}	total quantity of Bcd protein in the embryo, equivalent to total quantity of Dronpa-Bcd in bcd^{E1}embryos
Q_{app}	total quantity of bright state Dronpa-Bcd under conditions of optically augmented degradation
Q_{mat}/Q_{imm}	quantity of mature/immature Dronpa-Bcd in the embryo
$Q_{focal}/Q_{obscure}$	quantity of mature Dronpa-Bcd inside/outside the visible region of integration at the embryo surface, $Q_{mat} = Q_{focal} + Q_{obscure}$
Q_{bf}/Q_{df}	quantity of bright-state/dark-state Dronpa-Bcd in the region of integration at the embryo surface, $Q_{focal} = Q_{bf} + Q_{df}$
$G(\vec{r}, t)$	fraction of mature Dronpa-Bcd in the dark state at all points and times in the embryo
γ	fraction of mature Dronpa-Bcd located in the region of integration at the embryo surface, $\gamma = {}^{Q_{focal}}/_{Q_{mat}}$
$p(t)$	Dronpa-Bcd synthesis function
k_{mat}	rate of maturation of Dronpa chromophore
$m(t)$	newly maturing Dronpa-Bcd function, $m(t) = k_{mat}Q_{imm}$
S_{focal}	integration of I_{fluor} over embryo surface region
$C_{Dronpa-bright}$	contribution to I_{fluor} representing specific signal, the concentration of bright state Dronpa-Bcd
A	contribution to I_{fluor} representing autofluorescence
Φ (Φ_{dark})	flux of mature (dark-state) Dronpa-Bcd into the region of integration, $\Phi = \Phi_{bright} + \Phi_{dark}$
U	fraction of newly matured Dronpa-Bcd that appears initially in the dark state
δ/δ_a	duration of major/minor dark conversion series, $\delta = 13$ s, $\delta_a = 7$ s

k_{inc}	rate of incidental or spontaneous reactivation of Dronpa
k_{deg}	rate of Dronpa-Bcd degradation
τ_{Bcd}	Bcd protein lifetime, $\tau_{Bcd} = {}^{1}/_{k_{deg}}$
k_{simp}	rate of Dronpa-Bcd degradation assuming $\Phi = 0$

S2 Description of Dronpa photophysics

Reversibility of photoconversion and near-bistability of fluorescent and induced non-fluorescent states make Dronpa an especially suitable fluorophore for measuring degradation (19). As shown in Fig. 5 of Ref. (19), it has a deprotonated fluorescent state (B), which absorbs photons at 503 nm and reemits at 518 nm with a high fluorescence quantum yield of 0.85. We refer to B as the Dronpa "bright" or "on" state. With a relatively small cross-section, molecules excited at 496 nm are photoswitched to a protonated state (A_2), which has a minor absorbance peak at 388 nm, but is for our purposes nonfluorescent. We refer to A_2 as the Dronpa "dark" or "off" state. Fluorophores in the dark state are returned to the bright state with a comparatively large cross-section by illumination with 405 nm light. Thermal conversion to the bright state in the absence of light is also reported, though reported metastable lifetimes vary from 840 min. (27) to several days (Ref. (19) and Fig. 1e). There is an additional nonfluorescent protonated state (A_1) whose occupancy is determined by the solution pH. At pH 7.4, approximating physiological values, 0.4% of Dronpa molecules are in state A_1 (28). As such, A_1 is a negligibly small reservoir. Finally, there is a triplet dark state (D) which causes intermittent blinking of the fluorophores. This state is cycled back to the bright state with lifetime 15 s^{-1} and does not significantly distort measurements of the quantity of fluorophores transferred to the dark state over conversion series of the duration used in the experiment.

S3 Identification of image masks and computation of S_{focal}

We use a phase symmetry calculation function ("phasesym.m") from a MATLAB (The MathWorks, Natick, MA) computer vision library (29) to score the composite fluorescence image of the embryo at the mid-sagittal plane (Fig. S1a). The phase symmetry image is then thresholded to identify the vitelline membrane. The resulting mask is filled to determine the embryo mask, and this mask is then eroded with a disk structuring element of diameter corresponding to 14 μm. This gives a total of three masks identifying the embryo, the vitelline membrane, and the yolk, respectively. To calculate S_{focal}, we create a cortical mask, consisting of the region that belongs to the embryo mask but not to the vitelline mask or to the yolk mask (Fig. S1b). We integrate over the cortex alone rather than the entire embryo as including fluorescence from the yolk only reduces the signal-to-noise ratio of the measurement. As S_{focal} is intended to be a measure of quantity of fluorescent molecules rather than concentration, it remains to multiply fluorescence intensity measurements in the cortical mask, which are proportional to fluorophore concentration, by the volume they represent. Practically, this means that cortical intensity measurements must be weighted by their distance r from the anterior-posterior (A-P) axis, since

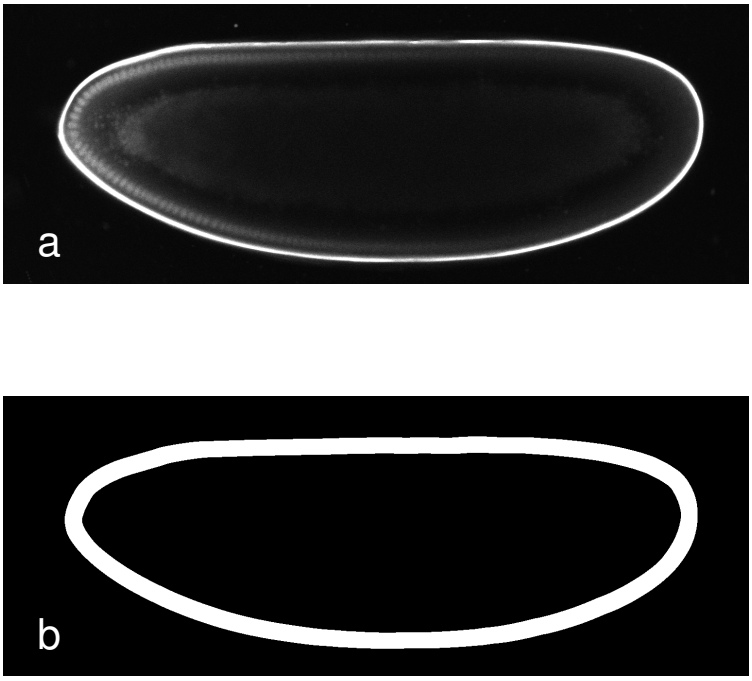

Figure S1: **Example of cortical mask selection for degradation rate measurement** a) Image of green channel fluorescence intensity (I_{fluor}) of a Dronpa-Bcd expressing embryo in mid-cycle-14. b) Cortical mask selected by eroding an embryo mask created after identifying the vitelline membrane by computer vision methods (see section S3). This mask is rotated around the A-P axis to create a volume of revolution which represents the region of integration for S_{focal}, or the volume within approximately 14 μm of the embryo surface.

we assume that the embryo has azimuthal symmetry. To determine the A-P axis, we find the maximal line segment that can be inscribed on the previously calculated embryo mask. We then subdivide the cortical mask into 400 boxes of approximately equal size using the prolate spheroidal coordinate system (as used in Ref. (30)), with the dorsal and ventral sides containing 200 boxes each. Rather than performing a explicit pointwise integration between $R_{min}(l)$ and $R_{max}(l)$, we instead find the mean radius $\bar{R}(l)$ for A-P axis position l of each box by calculating the distance between the centroids of corresponding dorsal and ventral boxes. Similarly, we find the mean fluorescence intensity $\bar{I}_{fluor}(r, l)$ in each box of the cortical mask. The integration of S_{focal} over r is then performed by trapezoidal rule and the integration over l by Riemann sum.

S4 Determination of Q_{bf} from S_{focal} time series

Because imaging alone is sufficient to photoconvert Dronpa-Bcd, simple identification of fluorescence intensity with initial bright state fluorophore concentration introduces error. Such errors become significant if small differences in intensity are used to compute derived quantities, as is the case in degradation rate measurements. A better approach is to acquire a time series of images and determine the initial fluorophore quantity by extrapolating backwards. Similarly, extrapolating forwards provides a measurement of the final fluorophore quantity.

$$S_{focal}(n) = \int C_{Dronpa-bright}(\vec{r}, n)d\vec{r} + A(n) \tag{S1}$$

$$= \int C_{Dronpa-bright}(\vec{r}, 0)e^{-k_{off}n}d\vec{r} + A(n) \tag{S2}$$

$$= e^{-k_{off}n}Q_{bf}(0) + A(n) \tag{S3}$$

The mean time series of autofluorescent signal A is measured by imaging wild-type (Oregon-R) embryos under the same experimental conditions as Dronpa-Bcd embryos, and is subtracted from S_{focal}. We then use a weighted least squares fitting method to extrapolate the original amount of bright state Dronpa-Bcd $Q_{bf}(0)$ and the final amount after the conversion series $Q_{bf}(t = \delta)$. We find that variance in the degradation rate measurement is minimized by setting the weights of all time points but the first and last equal to zero; this approach is optimal if error is dominated by variation in k_{off}. However, we find that the result is substantially identical if all weights are chosen to be equal.

An example of this fitting procedure is shown in Fig. S2b. The value of k_{off} used in the fit is adjusted for laser power fluctuations based on the linearity established in Fig. 2d. Experimentally, we use a series of 16 496 nm scans intensity averaged into 8 images for this measurement. If the conversion series immediately follows a complete activation sequence with 405 nm light, then we assume $Q_{focal}(0) = Q_{bf}(0)$. If the activation sequence is not complete, then a correction for the residual dark state amount is added, as described in Materials and Methods.

S5 Verification of uniformity of photoconversion

Ideally Dronpa-Bcd will be photoconverted uniformly throughout the embryo, to avoid equilibration between variably converted regions masking the effect of degradation. Lipid droplets in the embryo (31) inhibit imaging beyond the surface layer of the embryo on the side facing the objective, though they may only impede emission collection rather than absorption.

Let $G(\vec{r}, t)$ be the fraction of mature fluorophore in the dark state at all points in the embryo: $G(\vec{r}, t)$=$C_{Dronpa-dark}(\vec{r}, t)/C_{Dronpa}(\vec{r}, t)$. This quantity changes in time as new synthesis affects the bright and dark state populations asymmetrically. We consider simply $G_0(\vec{r})$, the profile of the conversion percentage G obtained after a single conversion series of 16 scans at 496 nm, assuming all fluorophore begins in the bright state.

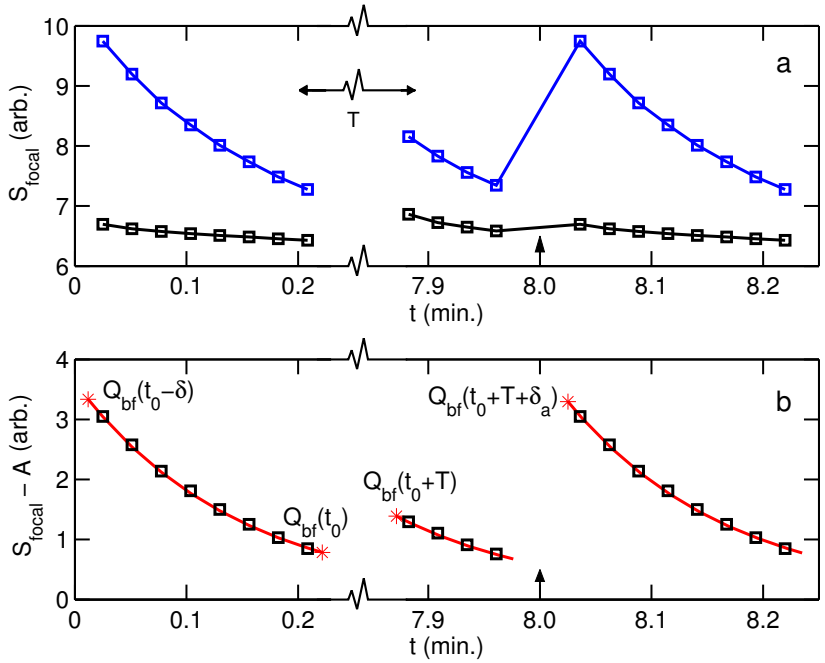

Figure S2: **Description of photoconversion quantity calculation** a) Integrated fluorescence intensity S_{focal} at the embryo surface, for a Dronpa-Bcd expressing embryo (blue) and an Oregon-R wild-type embryo (black, also denoted as autofluorescence level A). Each square represents integrated fluorescence for a single image, which is produced by averaging two individual scans. T indicates waiting interval duration, which is 8 minutes in this example. Arrow indicates the time of 405 nm reactivation pulse. b) Integrated fluorescence intensity after background subtraction, $S_{focal} - A$, indicated by black squares. Actual endpoints of each conversion series (red asterisks) indicate the quantity of bright state Dronpa-Bcd Q_{bf} at various times and are extrapolated assuming a single conversion rate k_{off}, determined as in Fig. 2b. Differences between these endpoints are used to calculate amount of Dronpa-Bcd transferred to the dark state, $Q_{df}(t_0)$, and amount of Dronpa-Bcd recovered from the dark state, $Q_{df}(t_0 + T)$, after a minor correction for residual dark state Dronpa from incomplete Dronpa reactivation (Eq. 11).

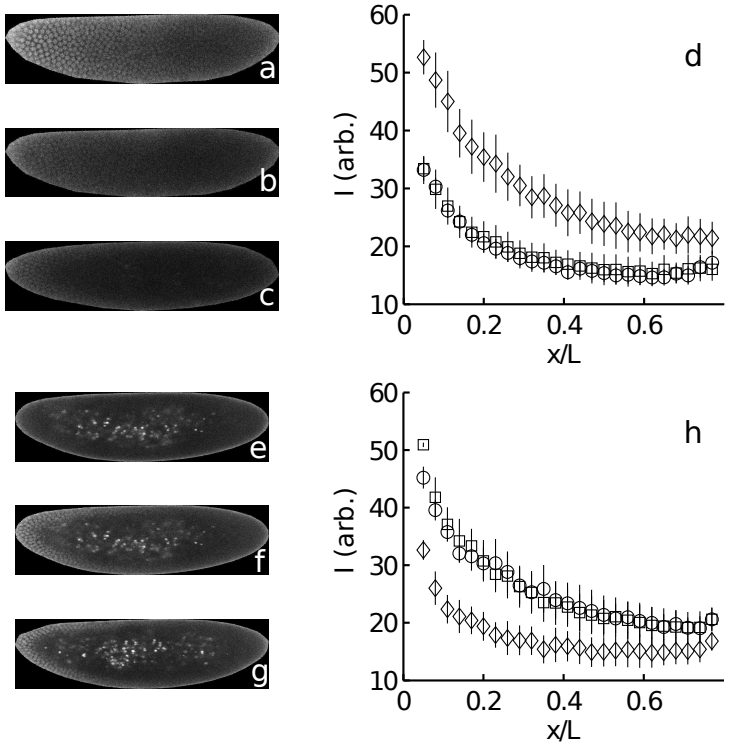

Figure S3: **Transparency of embryo to 496 nm and 405 nm photoconversion** a) Obverse face of embryo 60 μm above mid-sagittal plane prior to photoconversion b) Same as (a) post-photoconversion c) Reverse face of embryo 60 μm above mid-sagittal plane post-photoconversion d) Mean intensity gradients acquired from images in (a-c) for a set of 5 embryos. (a) diamonds, (b) squares, (c) circles. Error bars represent standard error. e) Obverse face of embryo 60 μm above mid-sagittal plane prior to photoactivation f) Same as (e) post-photoactivation g) Reverse face of embryo 60 μm above mid-sagittal plane post-photoactivation h) Mean intensity gradients acquired from images in (e-g) for a set of 3 embryos. (e) diamonds, (f) squares, (g) circles.

To determine the spatial dependence in $G_0(\vec{r})$, we acquire a fluorescence image on the obverse face of an embryo (Fig. S3a), followed by a 496 nm photoconversion series at the mid-sagittal plane, followed by a second image at the original location (Fig. S3b). The slide is then flipped over and the reverse side of the embryo is imaged at the same distance from the mid-sagittal plane (Fig. S3c). Intensity gradients extracted for an ensemble of embryos pre- and post-conversion are shown in Fig. S3d, indicating that the obverse and reverse face gradients are indistinguishable. We assume that Dronpa-Bcd in the yolk of the embryo is photoconverted in the same way, and take spatial inhomogeneities in G_0 to be negligible. If degradation and synthesis occur in equal proportion throughout the embryo as well, then $G(\vec{r}, t) = G(t)$ in general.

Additionally we require that 405 nm photoactivation be applied uniformly to the entire embryo. Although the delay between 496 nm images pre- and post-activation is too short for diffusion to be a concern, we want to be able to do multiple degradation experiments in a single embryo while avoiding accumulation of dark state fluorophore. To measure transparency we first apply a 496 nm photoconversion series at the mid-sagittal plane to populate the dark state. This is followed by a 496 nm image at the obverse (Fig. S3e), a 405 nm photoactivation pulse at the mid-sagittal plane, a second 496 nm image at the original location (Fig. S3f), and finally a 496 nm image on the reverse side at the same distance from the mid-sagittal plane (Fig. S3g). Fig. S3h shows that the intensity gradients extracted from the obverse and reverse sides are indistinguishable following the 405 nm pulse.

S6 Relation of total Bcd quantities to measured fluorescence values

We assume that the concentration of bright state Dronpa-Bcd in the focal volume is linearly proportional to fluorescence intensity when corrected for excitation power variation. However, to obtain measurements of Bcd synthesis and degradation, the true quantity of interest is the amount of Dronpa-Bcd in a closed volume rather than concentrations of fluorophore. While the entire egg is guaranteed to be a closed volume, for technical reasons we are unable to image the egg in its entirely. Rather, we use a region of integration at the embryo surface as the closed volume, and attempt to quantify the amount of Bcd flux that violates this assumption.

The total quantity of Bcd in the egg, Q_{Bcd}, has mature and immature components: $Q_{Bcd} = Q_{mat} + Q_{imm}$. Assuming first-order kinetics, these quantities evolve according to the following equations:

$$\frac{\partial Q_{Bcd}}{\partial t} = p(t) - k_{deg} Q_{Bcd} \tag{S4}$$

$$\frac{\partial Q_{imm}}{\partial t} = p(t) - k_{mat} Q_{imm} - k_{deg} Q_{imm} \tag{S5}$$

$$\frac{\partial Q_{mat}}{\partial t} = k_{mat} Q_{imm} - k_{deg} Q_{mat} \tag{S6}$$

$p(t)$ represents the rate of synthesis of new protein, and k_{mat} and k_{deg} are the rates of maturation and degradation, respectively. Measurement of the maturation lifetime of Dronpa *in vivo*

is beyond the scope of this work, and Q_{imm} cannot be measured; therefore, we combine these quantities into $m(t) = k_{mat}Q_{imm}$ to simplify the equations:

$$\frac{\partial Q_{mat}}{\partial t} = m(t) - k_{deg}Q_{mat} \tag{S7}$$

Only a fraction of the total mature fluorophore will be located such that its emission will be observed in the focal region of a confocal microscope. This is distinguished from the question of absorption of incident light, because while scattered photons from the excitation beam may be absorbed far from the focus, their emission signal will be excluded by the confocal pinhole. As mentioned previously, the *Drosophila* embryo is known to contain a distribution of yolk granules as well as lipid droplets which are rearranged in a controlled fashion during the mitotic division cycles prior to gastrulation (31). These droplets scatter light in visible wavelengths and affect the size of the region of the embryo observable under fluorescence microscopy. The total quantity of mature Dronpa-Bcd thus breaks down into that which is observable and located in our region of integration (Q_{focal}) and that which is not ($Q_{obscure}$), such that $Q_{mat} = Q_{focal} + Q_{obscure}$:

$$\frac{\partial Q_{focal}}{\partial t} = m(t)\gamma_{imm}(t) - k_{deg}Q_{focal} + \Phi(t) \tag{S8}$$

$$\frac{\partial Q_{obscure}}{\partial t} = m(t)(1 - \gamma_{imm}(t)) - k_{deg}Q_{obscure} - \Phi(t) \tag{S9}$$

We let $\Phi(t)$ denote the flux of mature fluorophore into the region of integration, comprising the effect due to both the actual transport of fluorophores and the resizing of the observable region. Φ is a potentially significant quantity as a nonzero value invalidates the assumption that the region of integration is a closed volume, introducing an error into our attempt to measure the degradation. $\gamma_{imm}(t)$ represents the fraction of total immature fluorophore located in the focal region. For simplicity, we assume that both immature and mature fluorophore is distributed between the observable and obscure regions in the same way, making the substitution $\gamma_{imm}(t) = \gamma_{mat}(t) = \gamma(t)$. Hence $Q_{focal} = \gamma(t)Q_{mat}$ and $Q_{obscure} = (1 - \gamma(t))Q_{mat}$. Subsequently:

$$\frac{\partial Q_{focal}}{\partial t} = \gamma(t)\left[m(t) - k_{deg}Q_{mat}\right] + \Phi(t) \tag{S10}$$

$$= \gamma(t)\frac{\partial Q_{mat}}{\partial t} + \Phi(t) \tag{S11}$$

$$\frac{\partial Q_{obscure}}{\partial t} = (1 - \gamma(t))\left[m(t) - k_{deg}Q_{mat}\right] - \Phi(t) \tag{S12}$$

$$= (1 - \gamma(t))\frac{\partial Q_{mat}}{\partial t} - \Phi(t) \tag{S13}$$

However, by chain rule we also obtain $\dot{Q}_{focal} = \gamma\dot{Q}_{mat} + \dot{\gamma}Q_{mat}$ and so we can simply replace $\Phi(t)$ with $\Phi(t) = \dot{\gamma}(t)Q_{mat}$. This quantity will be used in section S8 to correct for flux after obtaining estimates of $\gamma(t)$.

S7 Correction for Dronpa-Bcd flux

In the simplest interpretation of our data, the rate of Dronpa-Bcd degradation k_{deg} can be directly inferred from the quantities of dark state fluorophore measured at times t_0 and $t_0 + T$. Let k_{simp} be the degradation rate measured according to the assumption that $\Phi = 0$.

$$k_{simp} = \frac{log\left(Q_{df}(t_0)\right) - log\left(Q_{df}(t_0 + T)\right)}{T} \tag{S14}$$

Allowing nonzero flux of dark state fluorophore into the focal region Φ implies that $k_{deg} \neq k_{simp}$. However, with an estimate of $\Phi(t)$ we can solve for k_{deg}.

Removing terms denoting thermal reactivation of Dronpa and maturation into the dark state, both of which are negligible, Eq. 8 becomes

$$\frac{\partial Q_{df}}{\partial t} = -k_{deg} Q_{df} + \Phi_{dark}(t) \tag{S15}$$

which is solved by

$$Q_{df}(t) = \int_{t_0}^{t} e^{-k_{deg}(t-t')} \Phi_{dark}(t') dt' + Q_{df}(t_0) e^{-k_{deg}(t-t_0)} \tag{S16}$$

We then note that this can be further simplified:

$$\frac{Q_{df}(t)}{Q_{df}(t_0)} = e^{-k_{deg}(t-t_0)} \left(\int_{t_0}^{t} e^{k_{deg}(t'-t_0)} \frac{\Phi_{dark}(t')}{Q_{df}(t_0)} dt' + 1 \right) \tag{S17}$$

$$= e^{-k_{deg}(t-t_0)} \left(\int_{t_0}^{t} \frac{\dot{\gamma}(t')}{\gamma(t_0)} dt' + 1 \right) \tag{S18}$$

where in the integral we have made use of the fact that $Q_{dark}(t') = Q_{dark}(t_0) e^{-k_{deg}(t'-t_0)}$. We can solve explicitly for the degradation rate, now corrected for flux:

$$k_{deg} = -\frac{1}{T} log\left(\frac{Q_{df}(t_0 + T)}{Q_{df}(t_0)}\right) + \frac{1}{T} log\left(\int_{t_0}^{t_0+T} \frac{\dot{\gamma}(t')}{\gamma(t_0)} dt' + 1 \right) \tag{S19}$$

$$= k_{simp} + \frac{1}{T} log\left(\int_{t_0}^{t_0+T} \frac{\dot{\gamma}(t')}{\gamma(t_0)} dt' + 1 \right) \tag{S20}$$

Eq. S20 is used in Fig. 4e to obtain curves of k_{deg} after correction for each estimate of monotonic flux.

S8 Estimation of Dronpa-Bcd flux correction

As shown in section S6, $\Phi(t)$ is given by $\dot{\gamma}(t)Q_{mat}$, and can be determined exactly if the fraction of fluorophore in the observable region γ is known at all times. We can estimate γ indirectly by measuring the distribution of Dronpa-Bcd between cortex and core in fixed embryonic cross-sections. Additionally, though we cannot obtain an absolute value for γ, we can estimate the relative change in γ, or $\dot{\gamma}/\gamma$, by measuring the time evolution of Q_{focal} for fluorescently-tagged histone, H2A-RFP. The relative change $\dot{\gamma}/\gamma$ is all that is necessary to compute the correction to the degradation rate measurement, as shown in Eq. S20.

We fix 100 Dronpa-Bcd expressing embryos of various ages less than 3 hours post-oviposition and slice them in cross-sections transverse to the A-P axis. We acquire images of specific Dronpa-Bcd fluorescence by using 405 and 496 nm illumination to switch between Dronpa bright and dark states, and then subtract consecutive images. These images are computationally segmented into 14 annuli of maximum radius r, and the fraction of Dronpa-Bcd in each annulus, $Q(r)/\Sigma Q$, is calculated. A uniform distribution of Dronpa-Bcd will give $Q(r)/\Sigma Q \propto r$. We then stage the slices according to mitotic cycle by inspection, and estimate $\gamma(t)$ by summing the values in the outermost annuli, corresponding to the surface region of integration. The result of this experiment is illustrated in Fig. 4d.

Though it is believed that all histones necessary for the pre-gastrula are present at fertilization and stored in lipid droplets until they become needed after several cycles of DNA replication (32), an increase in the observed intensity of RFP-tagged histone is nevertheless observed when imaging embryos in the mitotic cycles prior to gastrulation under confocal microscopy. Many of the same factors that effect an increase in intensity of fluorescently tagged histone, such as clearing of the cortical cytoplasm, movement of nuclei to the cortex, and changes in pH, also impact the intensity of fluorescently tagged Bcd. Combined with the supposition that the quantity of histone molecules is constant with no new synthesis from translation of maternal RNA, it seems reasonable to consider H2A-RFP intensity as a proxy for determining $\dot{\gamma}/\gamma$. We use embryos for which part of the maternally deposited H2A is conjugated to RFP and measure surface intensity S_{focal}, here using the red rather than the green channel, by the method of section S3. The background value A is determined by an identical measurement of Oregon-R embryos. As there is negligible photoconversion of H2A-RFP, we assume $Q_{focal} \propto S_{focal} - A$ for a series of time points spaced over the mitotic cycles prior to gastrulation, and assume that all change in Q_{focal} is due to redistribution of fluorophore or changes in the opacity of the surface region. The relative change in γ, $\dot{\gamma}/\gamma$, can be directly extracted given these assumptions.

S9 Removal of cell-cycle-periodic oscillation

To arrive at a value of k_{deg} corrected for cell-cycle-periodic oscillations but not for any monotonic flux, we assume that $\gamma(t) = 1 + Csin(\omega t + \phi)$, where ω is the frequency of mitotic divisions. This will describe a general sinusoidal flux of a single frequency. For single-exponential

decay, this will give

$$\frac{Q_{df}(t+T)}{Q_{df}(t)} = e^{-Tk_{deg}(t)}\left[\frac{1+Csin\left(\omega(t+T)+\phi\right)}{1+Csin\left(\omega t+\phi\right)}\right] \tag{S21}$$

The bracketed term oscillates with period $2\pi/\omega$. We eliminate the periodic oscillation as follows: a linear least squares fit is performed on the curves $f(t) = Q_{df}(t+T)/Q_{df}(t)$ for waiting intervals T = 4, 8, and 15 minutes. The curves are then de-trended, by removing any linear trend as determined by least-squares fit, and decomposed into Fourier vectors. We remove Fourier components with period greater than 12 minutes, which is the approximate length of mitotic cycles 12 and 13. The Fourier transform is then inverted and the linear trend reintroduced to give an adjusted $\widetilde{f}(t)$ with cell-cycle-periodic oscillations removed, from which the corrected degradation rate can be directly extracted.

S10 Measurement of total Bcd protein by Western blot

We extracted total protein from embryos that develop within consecutive 30 minute time windows following fertilization. More than 95% of embryos collected in this way are within the predicted 30 minute time window as determined by scoring the onset of cephalic furrow formation. Anti-GFP antibody is a mixture of two mouse monoclonal antibodies purchased from Roche (Cat# 11 814 460 001) used 1:100 in 1xPBS, 0.1% Tween 20, and 10% non-fat dry milk for ~3 hours at room temperature. The relative amounts of Bcd are then established by detecting a chemi-luminescent signal with a CCD camera (33). Shown in Fig. 5a is a typical western blot and, in Fig. 5b, the quantification of 5 different experiments that represent a total of 400 embryos per lane. By measuring the integrated CCD intensity of known quantities of rGFP, we can calibrate the Bcd western blot to determine the absolute number of Bcd molecules in the embryo at each stage. Recombinant GFP (rGFP) was purchased from Clontech (Cat# 63 23 73). In Fig. S4 is plotted the intensity obtained for a variety of masses M of rGFP, which are well fit to a line that passes through the origin. This establishes linearity of protein mass with blot intensity in the regime tested, which includes the intensity corresponding to GFP-Bcd from early cycle 14 embryos.

S11 Measurement of gradient shift under optically-mimicked degradation

We determine the rate of apparent Dronpa-Bcd degradation induced by imaging at a given 496 nm laser power in units of 1/scans, as shown in Fig. S5. In contrast to the lifetime experiments, rapidity of photoconversion is not of primary importance; hence we use a lower excitation power and the conversion rate is not identical to that found in Fig. 2.

Having determined the rate of degradation added by photoconversion, we then mount embryos expressing Dronpa-Bcd as well as Histone-RFP on a slide along with embryos expressing only Histone-RFP (H2A-RFP), and image both groups in a looping sequence for 70 minutes.

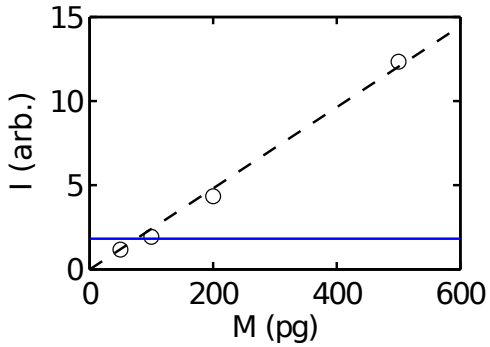

Figure S4: **Calibration of blot intensity to molecule count** Calibration of Bcd Western blots to absolute number of Bcd molecules. Circles indicate integrated CCD intensity of known masses M of rGFP, measured in picograms. Dashed line is a least squares fit of these points anchored to the origin. Blue line indicates integrated CCD intensity of GFP-Bcd at time point $t = 135$ min., which intersects the best-fit line at $M = 75$ pg of rGFP.

Fluorescence images in green (520-570 nm) and red (590-660 nm) channels are collected. For imaging Histone-RFP fluorescence, we use a 561 nm He-Ne laser at 40 μW. A distribution of optically augmented degradation rates is obtained by choosing a different total number of embryos over which to loop (N = 12, 16, 20, 28, and 36) for each slide, which effects a change in the scan frequency and, by extension, the rate of optically-augmented degradation.

After 70 minutes of images have been collected at the augmented optical degradation rate, a single loop of 405 nm scans is performed to reactivate all dark state Dronpa-Bcd in the embryo. Subsequently two additional imaging loops at 496 nm are performed. These two images are averaged for each embryo to determine the full Bcd gradient after Dronpa reactivation, and the two images of each embryo immediately prior to 405 nm reactivation are averaged to determine the gradient after equilibration to the optically-augmented degradation rate.

The nuclear concentration gradient for each embryo is determined by creating a nuclear mask in MATLAB using the red channel fluorescence image, which indicates the Histone-RFP signal (Fig. S6a). The fluorescence intensity in the red channel is thresholded to create an initial mask and the final nuclear mask is given by the union between the initial mask and the cortical mask calculated by the method described in section S3. An example of the resulting nuclear mask is shown in Fig. S6b.

Absolute Dronpa-Bcd intensity is determined in the following way. We divide the nuclear mask of each image into 200 boxes projected onto the A-P axis, and calculate the mean intensity in both green and red channels in each box. The mean green intensity in each box is then divided by the corresponding mean red intensity to effectively normalize the green signal by the DNA content. Smoothed green channel gradients from the Histone-RFP expressing embryos are then

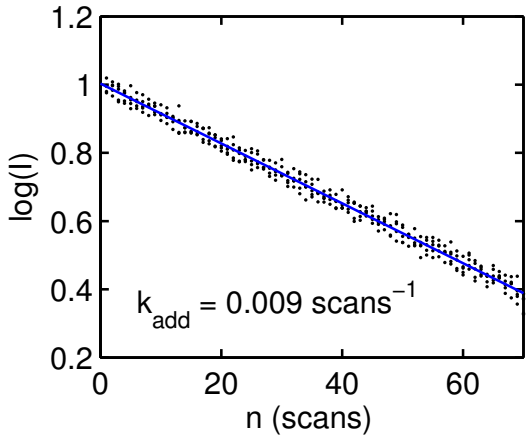

Figure S5: **Quantification of mimicked Dronpa-Bcd degradation induced by photoconversion** I indicates fluorescence intensity of a region containing highly Dronpa-Bcd expressing nuclei at the anterior of the embryo, after subtraction of Histone-RFP background. n indicates scan number. Blue line is a linear least-squares fit. In units of scan frequency, each scan augments fluorophore degradation by $k_{add} = 0.009$ scans^{-1}. Each 70 scan experiment takes less than 50 s, rendering the effect of endogenous degradation negligible.

subtracted from the Dronpa-Bcd/Histone-RFP gradients for which they are matched controls, as determined by identical scan frequency and pre-/post- activation classification.

In the one-dimensional synthesis-diffusion-degradation model with idealized source conditions (constant synthesis strictly located at the anterior tip), the equilibrium morphogen distribution takes the form of an exponentially decaying profile combined with a reflection due to the imposition of a no-flux boundary condition at the posterior end:

$$c = B\left(e^{-x/\lambda} + e^{x-2L/\lambda}\right) \tag{S22}$$

where c is the morphogen concentration, B is a constant, and λ is the characteristic length $\sqrt{D\tau}$. We fit the observed gradients to this equation using a least-squares method to quantify the change in characteristic length effected by the augmented degradation of the morphogen. We find a result that is qualitatively similar to that obtained from fitting to a more accurate model, incorporating a realistic source distribution, as shown in Fig. 6b, inset.

S12 Calculation of Bcd synthesis rate from Western analysis

Models that account for the dynamics of the Bcd gradient generally assume constant production of Bcd beginning at fertilization (7); however, existing evidence for this assumption is equivocal. On one hand, the mRNA encoding Bcd appears constant until cycle 14 when it decays (7, 34) (Fig. 5c). On the other, the dynamics of the polyA tail length suggest that synthesis of

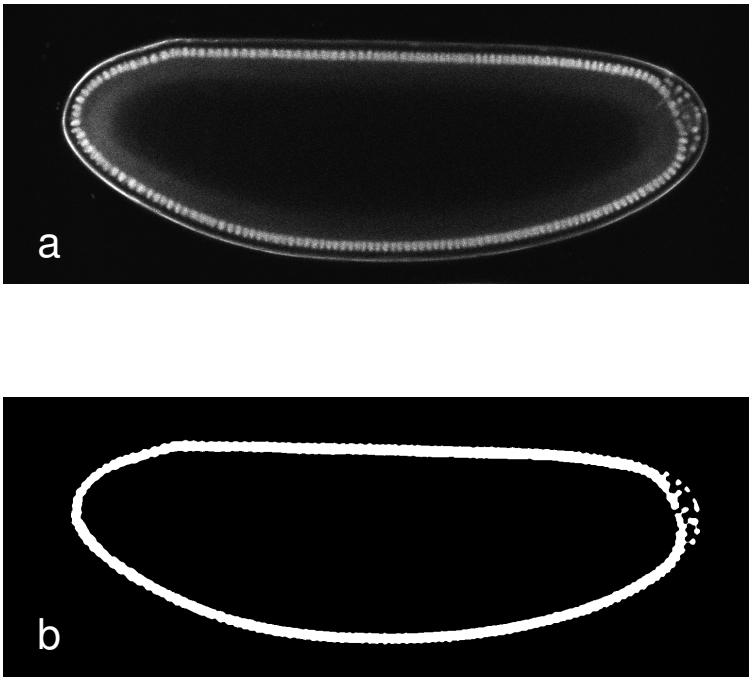

Figure S6: **Identification of nuclear mask for Bcd gradient computation** a) Image of red channel fluorescence intensity of a Dronpa-Bcd/H2A-RFP expressing embryo in mid-cycle-14. Red channel shows Histone-RFP fluorescence and negligible Dronpa-Bcd fluorescence. b) Nuclear mask selected by thresholding the image in (a) and taking the union with the cortical mask as calculated by the method described in section S3 and Fig. S1.

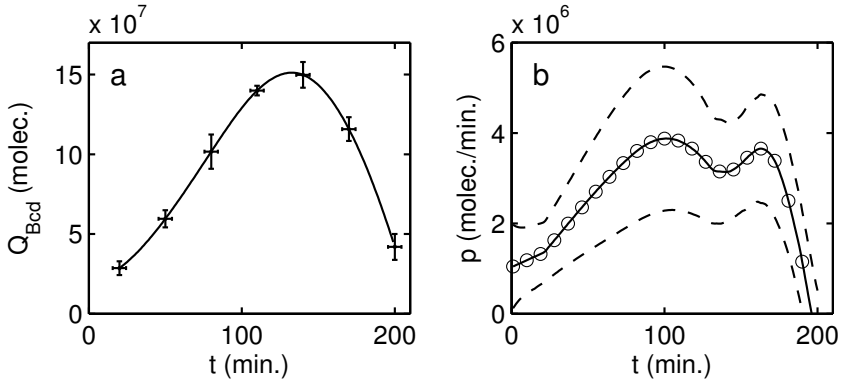

Figure S7: **Calculation of Bcd synthesis rate** a) Quantification of an ensemble of 5 Bcd Western blots (Fig. 5b). b) Production rate $p(t)$ of new Bcd protein implied by Bcd quantity in (a) and degradation rate time series in Fig. 4e, extended based on the assumption that $k_{deg} = 0.020$ min^{-1} prior to cycle 11 and smoothed by moving average to match time resolution of western blot. Production rate increases until cycle 14 and drops off to zero once gastrulation begins. Dashed lines indicate error as propagated from Q_{Bcd} and k_{deg}. Units indicate the number of Bcd molecules translated per minute.

Bcd might not be constant (22, 23). We perform two independent measurements that each indirectly reflect the synthesis rate of Bcd. One is the total accumulation of Bcd in the embryo over time, extracted from Western blotting, from which we can extract the production rate based on our measurement of Bcd degradation. The other is based on the appearance of new Dronpa-Bcd fluorescence after prior photoconversion, reflecting the rate of synthesis plus a delay dependent on the maturation time of the fluorophore.

If the overall amount of Bcd in the embryo changes according to

$$\frac{dQ_{Bcd}}{dt} = p(t) - k_{deg}Q_{Bcd} \tag{S23}$$

where $p(t)$ is the time-dependent synthesis of Bcd, k_{deg} the degradation rate, and Q_{Bcd} the total quantity of Bcd in the embryo, then, assuming that $k_{deg} = 0.020$ min^{-1} prior to cycle 14, and that Q_{Bcd} is as determined from Western blotting, we obtain the Bcd synthesis function, $p(t)$, shown in Fig. S7b. Though error bars are large, as this number is calculated from two independent quantities, we see a definite increase up to cycle 14. If we allow that the dynamics of the polyA tail of *bcd* mRNA could effect an increasing rate of protein synthesis even with a constant mRNA level, it is consistent with measurement of *bcd* mRNA by RT-PCR (Fig. 5c), which indicates relatively constant mRNA levels until cycle 14, followed by complete extinction in the gastrula.

S13 Measurement of newly maturing Dronpa-Bcd

Although we can infer the rate of synthesis of Bcd, $p(t)$, from our measurement of degradation and the quantification of total Bcd in the embryo (see section S12), we can also determine the amount of newly maturing Dronpa-Bcd from our experiments. The amount of newly matured Dronpa-Bcd is not equivalent to the amount of newly synthesized Dronpa-Bcd, as it is filtered through the Dronpa maturation process. However, we can verify that this measurement is consistent with a simple kinetic model incorporating our previously reported synthesis and degradation rates and a reasonable assumption for the *in vivo* Dronpa maturation lifetime.

Since our measurements give complete information about the evolution of dark state Dronpa-Bcd, we can use this to determine the fraction of the change in bright state fluorophore that is attributable to newly matured protein. As described previously, all newly matured Dronpa-Bcd appears in the bright state. No assumptions need to be made to correct for the possibility of fluorophore redistribution.

The mature fluorophore in the observable region is distributed into the bright and dark states of Dronpa:

$$\frac{\partial Q_{df}}{\partial t} = -k_{deg} Q_{df} + \Phi_{dark}(t) \tag{S24}$$

$$\frac{\partial Q_{bf}}{\partial t} = m(t)\gamma(t) - k_{deg} Q_{bf} + \Phi_{bright}(t) \tag{S25}$$

We can rewrite the last two terms in the equation for bright fluorophore evolution. Recall that $Q_{df} = G(t)Q_{focal}$ and correspondingly $Q_{bf} = (1 - G(t))Q_{focal}$.

$$\frac{\partial Q_{bf}}{\partial t} = m\gamma - k_{deg}(1-G)Q_{focal} + (1-G)\Phi \tag{S26}$$

$$= m\gamma + \frac{1-G}{G}\left(-k_{deg} G Q_{focal} + G\Phi\right) \tag{S27}$$

$$= m\gamma + \frac{Q_{bf}}{Q_{df}}\frac{\partial Q_{df}}{\partial t} \tag{S28}$$

Integration allows us to solve for the newly matured protein in the observable region:

$$\int_{t_0}^{t} m(t')\gamma(t')dt' = \int_{t_0}^{t} \frac{\partial Q_{bf}}{\partial t'}dt' - \int_{t_0}^{t} \frac{Q_{bf}}{Q_{df}}\frac{\partial Q_{df}}{\partial t'}dt' \tag{S29}$$

$$\cong Q_{bf}(t) - Q_{bf}(t_0) - \left[\frac{Q_{bf}(t) + Q_{bf}(t_0)}{Q_{df}(t) + Q_{df}(t_0)}\right]\left(Q_{df}(t) - Q_{df}(t_0)\right) \tag{S30}$$

We make the assumption that the change in fraction of dark state fluorophore G is small and use a linear approximation for ${}^{1-G}/_{G}$ (bracketed term). An estimation of the value of ${}^{m}/_{Q_{mat}}$ can be obtained by dividing out $Q_{focal} = \gamma Q_{mat}$.

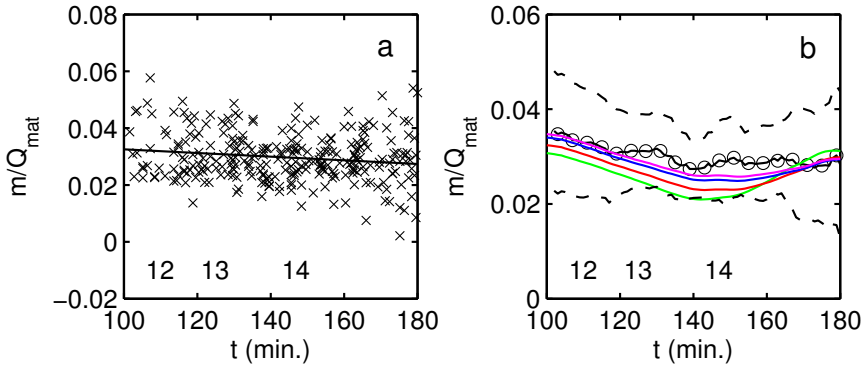

Figure S8: **Measurement of newly matured Dronpa-Bcd and agreement with simulation** a) Fraction of mature Dronpa-Bcd fluorophore newly matured within the past minute, $^{m}/_{Q_{mat}}$, in units of inverse minutes, for all $T = 8$ and 15 minute experiments. 4 minute experiments are too short to obtain precise measurements of new maturation. t is in minutes since fertilization, and the onset of each mitotic cycle is shown. Least squares fit indicated by solid line. b) $^{m}/_{Q_{mat}}$ from (a) (circles) input to moving average filter of span 13 minutes, with standard deviation indicated by dashed lines. Predicted value of $^{m}/_{Q_{mat}}$ obtained by simulation of our estimate of k_{deg} (Fig. 4e) and production time series $p(t)$ (Fig. S7b) extracted from Western blots, assuming that maturation and degradation are Poisson processes with maturation lifetime 10 minutes (green), 30 minutes (red), 100 minutes (blue), and 300 minutes (magenta).

In Fig. S8a, we show the fraction of mature Dronpa-Bcd fluorophore newly matured within the past minute, $^{m}/_{Q_{mat}}$, as calculated by this method. We fit this data to a line, which shows a negative trend in time, starting with a mean value of 0.033 min^{-1} at the midpoint of interphase 11 and decreasing to 0.027 min^{-1} at the end of interphase 14.

To verify that these values agree with the previously reported degradation and synthesis rates, we find a predicted value of $^{m}/_{Q_{mat}}$ assuming the egg is activated with zero Bcd protein and that maturation and degradation subsequently occur as Poisson processes. For the degradation rate we assume that $k_{deg} = 0.02$ min^{-1} prior to cycle 14 and increases within cycle 14 as indicated in Fig. 4e. We do not assume a constant production rate; we use the time-dependent function that we extract from our estimate of k_{deg} and Q_{Bcd} as determined by Western blot. This function, $p(t)$, is shown in Fig. S7b. Assuming a Dronpa maturation rate of 100 minutes or longer, we find that $^{m}/_{Q_{mat}}$ takes a time series that very closely approximates the measured value, as indicated in Fig. S8b. Shorter maturation lifetimes are less consistent with our data, but only those of 10 minutes or less yield values that fall outside one standard deviation of the measurement. This justifies our assumption of a 60 minute maturation lifetime used for simulations of gradient shape in Fig. 6b.

S14 Measurement of Bcd lifetime is insensitive to position along the anterior-posterior axis

As described in Section S6, the use of Dronpa photoconversion to measure protein degradation relies on the assumption that the region over which fluorophore concentration is integrated is a closed volume. In the earlier part of this chapter, the region of integration is taken to be the entire cortex or surface region of the embryo, extending the length of the A-P axis and penetrating 14 μm basally from the vitelline membrane. The core-to-cortex flux measured and corrected for in section S7 represents a deviation from this assumption. However, while there is reason to believe that flux of Bcd from core-to-cortex is significant, it is at least plausible that flux between surface regions along the A-P axis is negligible in later syncytial blastoderm stages, if hypotheses about compartmentalization of cortical cytoplasm (21) and small diffusion constants (3) in the cortical region are assumed.

With the assumption that exchange of Dronpa-Bcd between neighboring cortical A-P sections is negligible, it becomes possible to measure the Bcd degradation rate k_{deg} as a function of A-P axis position, $k_{deg}(x)$. Spatial inhomogeneities in k_{deg} could simply reflect differences in absolute Bcd concentration along the A-P axis, which would suggest a non-first-order degradation process. This has been hypothesized as a mechanism for creating gradients of shape other than exponential (35). Alternatively, the degradation mechanism might itself be variable with position, which is itself a conceivable mechanism for creating morphogen concentration gradients, and which has been observed in aspects of the *C. elegans* patterning system (36).

In Fig. S9b is shown the degradation rate, uncorrected for flux, calculated for various distinct regions of integration along the A-P axis (Fig. S9a). Error bars are of the same magnitude as in Fig. 4e and are not shown. However, error is dominated by embryo-to-embryo variation, suggesting that differences in degradation between regions, for the same set of embryos, are much more likely to be significant. Regardless, no significant difference is seen between the degradation rate calculated for the mid-anterior and posterior regions despite a difference in absolute concentration exceeding a factor of two, casting doubt on the hypothesis of second-order degradation (35). A slightly less pronounced cell-cycle-periodic oscillation is observed in the uncorrected degradation rate from the anterior-most region, which is potentially explained by the smaller surface area connecting this region to the basal cytoplasm and yolk as compared to the more posterior regions.

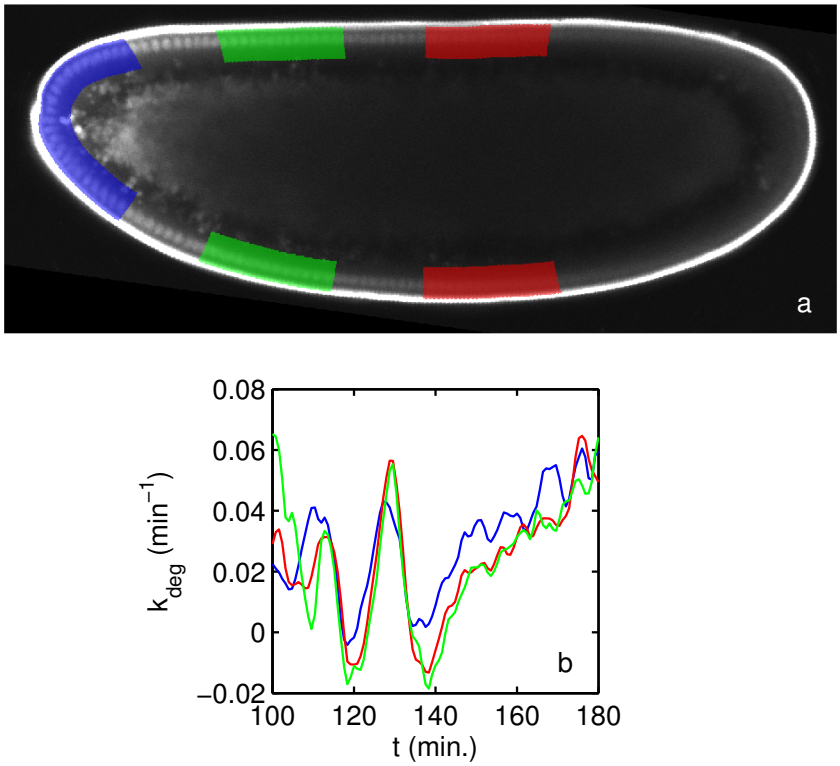

Figure S9: **Measurement of k_{deg} dependence on A-P axis position** a) Sample mid-cycle-14 embryo with three distinct regions of integration highlighted, at the anterior tip (blue), at the eventual cephalic furrow position (green), and immediately posterior of the embryo midline (red). As in Fig. S1, each mask is rotated around the A-P axis to create a volume of revolution which represents the region of integration for S_{focal}. b) $k_{simp}(x)$ calculated for each of the three regions in (a) as a function of time since fertilization. Measurements prior to cycle 14 are uncorrected for flux, either cell-cycle-periodic or monotonic. As in Fig. 4a, each solid line represents smoothing spline fit to all data smoothed by a Savitzky-Golay filter (26) of span 6.

27. Stiel, A. C., S. Trowitzsch, G. Weber, M. Andresen, C. Eggeling, S. W. Hell, S. Jakobs, and M. C. Wahl, 2007. 1.8 angstrom bright-state structure of the reversibly switchable fluorescent protein Dronpa guides the generation of fast switching variants. *Biochemical Journal* 402:35–42.

28. Habuchi, S., P. Dedecker, J. I. Hotta, C. Flors, R. Ando, H. Mizuno, A. Miyawaki, and J. Hofkens, 2006. Photo-induced protonation/deprotonation in the GFP-like fluorescent protein Dronpa: mechanism responsible for the reversible photoswitching. *Photochemical & Photobiological Sciences* 5:567–576.

29. Kovesi, P. D. MATLAB and Octave functions for computer vision and image processing. <http://www.csse.uwa.edu.au/˜pk/research/matlabfns/>. School of Computer Science & Software Engineering, The University of Western Australia.

30. Coppey, M., A. M. Berezhkovskii, Y. Kim, A. N. Boettiger, and S. Y. Shvartsman, 2007. Modeling the bicoid gradient: Diffusion and reversible nuclear trapping of a stable protein. *Developmental Biology* 312:623–630.

31. Welte, M. A., 2009. Fat on the move: intracellular motion of lipid droplets. *Biochemical Society Transactions* 37:991–996.

32. Cermelli, S., Y. Guo, S. P. Gross, and M. A. Welte, 2006. The lipid-droplet proteome reveals that droplets are a protein-storage depot. *Current Biology* 16:1783–1795.

33. Ghaemmaghami, S., W. Huh, K. Bower, R. W. Howson, A. Belle, N. Dephoure, E. K. O'Shea, and J. S. Weissman, 2003. Global analysis of protein expression in yeast. *Nature* 425:737–741.

34. Surdej, P., and M. Jacobs-Lorena, 1998. Developmental regulation of bicoid mRNA stability is mediated by the first 43 nucleotides of the 3' untranslated region. *Molecular and Cellular Biology* 18:2892–2900.

35. Wartlick, O., A. Kicheva, and M. Gonzalez-Gaitan, 2009. Morphogen gradient formation. *Cold Spring Harbor Perspectives in Biology* 1:a001255.

36. DeRenzo, C., and G. Seydoux, 2004. A clean start: degradation of maternal proteins at the oocyte-to-embryo transition. *Trends in Cell Biology* 14:420–426.